Relative contributions of anomalous heat fluxes and effective heat capacity to sea surface temperature variability

Naoya Takahashi[1], Kelvin J. Richards[1,2], Niklas Schneider[1,2], Malte F. Stuecker[1,2], H. Annamalai[1,2], and Masami Nonaka[3]

[1] International Pacific Research Center, School of Ocean and Earth Science and Technology, University of Hawai'i at Mānoa, Honolulu, HI, USA

[2] Department of Oceanography, School of Ocean and Earth Science and Technology, University of Hawai'i at Mānoa, Honolulu, HI, USA

[3] Japan Agency for Marine-Earth Science and Technology, Yokohama, Kanagawa, Japan

Corresponding author: Naoya Takahashi (naoyat@hawaii.edu)

Key Points:

- Relative contributions of mixed layer depth (MLD) anomaly to SST variability are investigated using the Flux Divergence Angle (FDA) metric.
- MLD anomalies tend to amplify SST anomalies in the extra-tropics, especially in eastern ocean basin, during the spring and summer seasons.
- The contribution of MLD anomalies in the extra-tropics during summer is more pronounced on seasonal timescales than on sub-monthly ones.

Abstract

Sea surface temperatures (SSTs) vary not only due to heat exchange across the air-sea interface but also due to changes in effective heat capacity as primarily determined by mixed layer depth (MLD). Here, we investigate seasonal and regional characteristics of the contribution of MLD anomalies to SST variability using observational datasets. We propose a metric called Flux Divergence Angle (FDA), which can quantify the relative contributions of surface heat fluxes and MLD anomalies to SST variability. Using this metric, we find that MLD anomalies tend to amplify SST anomalies in the extra-tropics, especially in the eastern ocean basins, during spring and summer. This amplification is explained by a positive feedback loop between SST and MLD via upper ocean stratification. In contrast, MLD anomalies tend to suppress SST anomalies in the eastern tropical Pacific. The MLD contribution in the summer hemispheres is more pronounced on seasonal timescales than on sub-monthly timescales.

Plain Language Summary

Sea surface temperatures (SST) is one of the important indicators as well as drivers of climate variability over the globe. SST varies not only due to changes in surface heat fluxes but also due to changes in effective heat capacity as mainly determined by mixed layer depth (MLD) anomalies. In this study, we propose a new metric called "Flux Divergence Angle (FDA)", which can quantify the relative contributions of MLD and surface heat flux anomalies to the SST variability. Using this metric, we find that the MLD anomaly tends to amplify the local SST variability in the extra-tropics (especially in the eastern ocean basins) and during spring and summer. On the other hand, MLD anomalies tend to suppress the SST variability in the eastern tropical Pacific. Changes in effective heat capacity in the summer hemispheres are more important for slower SST variability (e.g., for several months) than that for faster one (e.g., for several days).

1 Introduction

Sea surface temperature (SST) is one of the key metrics as well as drivers of climate variability over the globe. Surface heat flux (SHF) is known as the most fundamental factor causing local SST variations in most of the extra-tropics (Hasselmann 1976; Frankignoul and Hasselmann 1977). Mixed layer depth (MLD) is in turn another key factor determining the effective heat capacity of the ocean surface layer, which also affects local SST variations (e.g., Alexander et al., 2000; Alexander & Penland, 1996; Amaya et al., 2021; Morioka et al., 2011; Qiu & Kelly, 1993; Takahashi et al., 2021; Yamamoto et al., 2020; Yokoi et al., 2012). More specifically, positive SST anomalies can be caused without SHF anomaly, if there is shallow MLD anomaly with climatological heating (and vice versa). Therefore, not only the flux of heat across the air-sea interface is important, but also how this heat is re-distributed within the mixed layer.

Based on a mixed layer temperature budget from in-situ observations, previous studies have shown that shallow MLD anomalies can cause positive SST anomalies especially in spring and summer when MLD is shallow and climatological surface heating exists (Alexander et al., 2000; Alexander & Penland, 1996; Cronin et al., 2013; Elsberry & Garwood, 1978; Lanzante &

Harnack, 1983). A part of the role of MLD anomalies has been revealed, however, a global picture of the relative importance of MLD anomalies in SST variability is missing. In the present, we can assess details of the role of MLD using various global datasets of vertical oceanic properties, such as Argo float observations. For example, Tozuka et al. (2018) proposed a metric for the relative importance of SHF and MLD anomalies to frontogenesis and frontolysis respectively based on Argo float data, finding that seasonal variations of the horizontal gradient of MLD strongly contribute to the strength of the SST front. In the present study, we revisit the relative importance of MLD and SHF anomalies to SST variability and explore their seasonal and regional characteristics over the global oceans.

The key scientific questions are "How large is the contribution of MLD anomalies to SST variability compared to the contribution of SHF anomalies?" and "When/Where are they most important?". To answer these questions, we 1) propose a metric for quantifying the relative contributions of SHF and MLD anomalies to the month-to-month variations of local SST anomalies and 2) reveal their seasonal (e.g., summer *vs.* winter) and regional characteristics (e.g., tropics *vs.* extra-tropics). Furthermore, potential timescale dependences of their contributions are explored using high-temporal oceanic reanalysis datasets.

The remainder of the paper is organized as follows. In section 2, we describe the datasets used in this study, and propose a metric to quantify the relative contributions of SHF and MLD anomalies to local SST variability. In section 3, we present the results on seasonality, regionality, and timescale dependence of the relative contribution of MLD anomaly. In section 4, we summarize our results and discuss the role of MLD anomalies in major climate modes.

2 Datasets and Methods

2.1 Datasets

In this study, we utilize three variables; SST, SHF, and MLD. Each variable is obtained from observational data sources; CERES-EBAF (Loeb et al., 2018) for radiative fluxes, OAFlux (Yu et al., 2008) for turbulent heat fluxes, OISST (Reynolds et al., 2002) for SST, and IPRC-Argo products (http://apdrc.soest.hawaii.edu/projects/argo/) for MLD. MLD is defined as the depth at which density increases from 10-m to the value equivalent to a temperature decrease of 0.2 ˚C. All variables are monthly-averaged, for 15 years from January 2005 to December 2019. The horizontal resolution of all variables is 1 degree in both zonal and meridional directions. In the latter part of the section 3, we examine the timescale dependence of the relative contributions of MLD and SHF using 5-day mean variables from the SODA 3.4.2 ocean reanalysis dataset (Carton et al., 2018), which is forced by the ERA-Interim dataset (Dee et al., 2011). While the seasonality and regionality of the relative contributions in the SODA dataset are slightly different from those in the observational datasets (cf. Figs. 2 *vs.* S2 and Figs. 3 *vs.* S3), our main conclusions are not sensitive to these different data sources.

2.2 Metric to determine the relative contributions of SHF and MLD anomalies to local SST variability

Here, we propose a metric to quantify the relative contributions of SHF and MLD anomalies to local SST variability. We start to develop the metric from the simplified mixed layer temperature budget equation (Qiu & Kelly, 1993) considering only surface forcing:

$$\frac{\partial T}{\partial t} = \frac{Q}{\rho c_p H} + \varepsilon_o \,, \qquad (1)$$

where ρ is the density of sea water, c_p the specific heat capacity at constant pressure, H is MLD, and ε_o is the sum of contributions from all other oceanic processes (i.e., three-dimensional advection, entrainment, and diffusion) and the residual derived from unresolved processes and observational error. T is vertical mean temperature within the mixed layer. In this study, we assume that T is equivalent to SST. Q is the surface heat flux into the mixed layer (i.e., SHF) and calculated as the difference between net surface heat flux (Q_0) and penetrative SW radiation at the bottom of mixed layer (q_{pen}); $Q = Q_0 - q_{pen}$. The q_{pen} is calculated following Paulson & Simpson (1977). Hereafter, we focus on month-to-month SST variations and define anomalies of all variables as the deviations from the climatology at each grid point. Considering the heat budget equation for T anomalies, we can decompose the anomalies of the first term on the right-hand-side (rhs) of equation (1) into contributions from SHF and MLD anomalies (Morioka et al., 2010; Yokoi et al., 2012). We can rewrite the heat budget equation:

$$\frac{\partial T'}{\partial t} \sim \frac{Q'}{\rho c_p \bar{H}} - \frac{\bar{Q} H'}{\rho c_p \bar{H}^2} + \varepsilon_o{}', \qquad (2)$$

where overbars ($\bar{X}$) and primes (X') denote the seasonal climatology and anomalies, respectively. The first term on the rhs represents the contribution of the SHF anomaly (Q') acting on a constant MLD ($\bar{H}$) and the second term represents the contribution of the MLD anomaly (H') under climatological heating/cooling ($\bar{Q}$). We ignore second and higher order terms of the Taylor

Expansion in equation (2) (e.g., the non-linear contribution of both anomalies) because they are typically much smaller than the sum of the first two terms (~1/10), except in the Antarctic Circumpolar Current (ACC) region and the Labrador sea where the subduction zone of the Atlantic Meridional Overturning Circulation is located. The first two terms can explain more than 90 % of the total variances of the surface forcing term in most of the region (Fig. S1).

Next, we formulate a temperature variance budget equation (Boucharel et al., 2015; Guan et al., 2019; Santoso et al., 2010) by multiplying the SST anomaly (T') on both sides of equation (2):

$$T'\frac{\partial T'}{\partial t} = T'\left(\frac{Q'}{\rho c_p \bar{H}} - \frac{\bar{Q}H'}{\rho c_p \bar{H}^2} + \varepsilon_o{}'\right), \quad (3)$$

$$T'\frac{\partial T'}{\partial t} = \frac{1}{\rho c_p \bar{H}}\left(Q'T' - H'\frac{\bar{Q}}{\bar{H}}T'\right) + \varepsilon_o{}'T'. \quad (4)$$

The left-hand-side of the equations are equivalent to half of the time tendency of T' squared, hence we can diagnose the dominant processes that result in an increase or decrease of the T' variance. The reason why we employ the heat variance budget equation (Eq. 4) instead of the heat budget equation (Eq. 2) is that the role of surface forcing processes in the SST evolution can be captured by the variance budget equation.

As noted in section 1, Tozuka et al. (2018) proposed a metric for quantifying the relative contribution of horizontal gradients of SHF and MLD to the seasonal variation of frontogenesis. The method is analogous to the so-called "Turner angle" (Ruddick, 1983; You, 2002) which can be used to diagnose relative contributions of vertical gradients of temperature and salinity to double-diffusive convection. Here, following the basic concepts of these two studies, we define a new metric called Flux Divergence Angle (FDA; Θ), which quantifies the relative contributions of SHF and MLD anomalies to local SST variability:

$$\Theta = \tan^{-1}\left(Q_Q - Q_H,\ Q_Q + Q_H\right), \quad (5)$$

where

$$Q_Q = Q'T', \qquad Q_H = -H'\frac{\bar{Q}}{\bar{H}}T'.$$

The two indices of Q_Q and Q_H are a part of the equation (4), have the same unit of K*W/m^2, and represent the product of anomalies of SST and SHF (or the product of anomalies of SST and equivalent heat flux anomalies due to a MLD anomaly with climatological heating/cooling) . Positive and negative values of these indices represent that the heat flux anomalies amplify and dampen the local SST anomalies, respectively. Figures 1a to 1c are snapshots of SST, SHF, and MLD anomalies on June 2015. In addition, a snapshot of FDA on June 2015 is shown in Fig. 1d, calculated via equation (5) at each grid point. Figure 1f shows a two-dimensional histogram of all pairs of Q_Q and Q_H, showing that there is no apparent linear relationship between them.

Next, we illustrate the physical meaning of the FDA using a schematic in Figure 1e. When the FDA has a positive value, i.e., when the sum of Q_Q and Q_H is positive, the covariance of total surface forcing and SST anomaly is positive, so that the surface forcing term in equation (4) acts to amplify the local SST anomalies. This is referred to as "Growth" stage of the SST

158 evolution by surface forcing. Analogous, when the FDA has a negative value, i.e., when the sum
159 of Q_Q and Q_H is negative, the covariance of total surface forcing and SST anomaly is negative, so
160 that the surface forcing term in equation (4) acts to dampen the local SST anomalies ("Decay"
161 stage). Additionally, when the relative contribution of SHF is larger than that of MLD, FDA has
162 a specific value range of $0° < \Theta < 90°$ for the "Growth" stage and $-180° < \Theta < -90°$ for
163 the "Decay" stage. In contrast, when the contribution of MLD is larger than that of SHF, FDA
164 has the range of $90° < \Theta < 180°$ for the "Growth" and $-90° < \Theta < 0°$ for the "Decay" stage.
165 Depending on the relative importance, we add the header of "Q_Q" or "Q_H" before the name of
166 "Growth" or "Decay" stage, e.g., "Q_Q Growth" when $0° < \Theta < 90°$. Note that a term of
167 "dominant" in the following text indicates their relative importance of the SHF and MLD terms
168 but not necessarily their absolute importance relative to other terms in the full variance heat
169 budget. For example, upwelling and lateral advection have large impacts on SST variability in
170 the eastern tropical Pacific and in western boundary current regions, respectively. In such cases,
171 surface forcing processes are less important than oceanic processes. Hence, the term "dominant"
172 used in this manuscript refers to only the relative importance of the SHF anomaly or MLD
173 anomaly among the surface forcing processes.
174

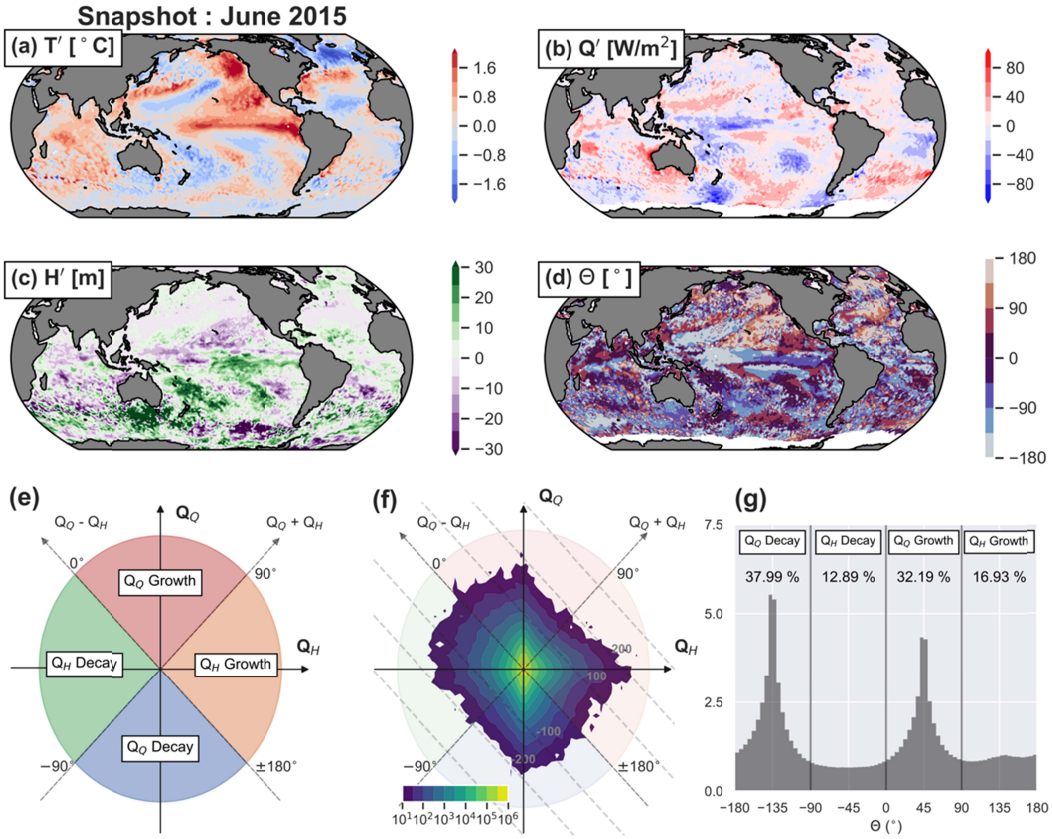

Figure 1 : Snapshots of horizontal maps of (a) SST anomaly, (b) SHF anomaly, (c) MLD anomaly, and (d) FDA on June 2015. (e) Schematic diagram of the four sectors ("Q_Q Decay"/ "Q_H Decay" / "Q_Q Growth" / "Q_H Growth") diagnosed by the FDA metric. (f) Two-dimensional histogram of Q_Q and Q_H using all pairs over the global ocean and in all seasons. Units of Q_Q and Q_H are K*W/m^2. Bin size is 10 K*W/m^2 for both Q_Q and Q_H. Only count numbers greater than 10 are displayed. Dashed contours where Q_Q+ Q_H =-300, -200, -100, 0, 100, 200, 300 are also plotted. (g) Histogram of FDA normalized by total count numbers (Unit: %) using a bin size of 5°. Numbers below each label indicate the occurrence frequency in each sector (Unit: %).

To further investigate the regional characteristics of the FDA histogram (Fig. 1g), we calculate the occurrence frequencies of the four sectors (F_i) at each grid point during specific seasons as below,

$$F_i(x,y) = \frac{N_i(x,y)}{N_{ALL}}, \qquad \begin{cases} i=1: & -180° \le \Theta < -90° \\ i=2: & -90° \le \Theta < 0° \\ i=3: & 0° \le \Theta < 90° \\ i=4: & 90° \le \Theta < 180° \end{cases} \tag{6}$$

where N_i is the count number of events with a specific value range of FDA. N_{ALL} is the total count number at each grid point, which is 45 for each season (i.e., each 3-month seasonal average during 15 years). Horizontal maps of F_i tell us the regionality of the dominant processes for the local SST evolution at each grid point.

3 Results

3.1 Global characteristics of FDA

First, we provide an overview of the general characteristics of the FDA using all pairs of Q_Q and Q_H over the global ocean and in all seasons. Figure 1g shows a histogram of FDAs normalized by total count numbers. The number below each label in Figure 1g indicates the occurrence frequency of each sector. The histogram has two sharp peaks at around 45˚ and -135˚. The occurrence frequency of "Q_Q Growth" is 32.19 % and that of "Q_Q Decay" is 37.99 %. These results demonstrate that SHF anomalies are the main factor determining anomalies of the total surface forcing term. This is consistent with previous results on the relationship between SHF and SST, i.e., SST anomalies can be caused by wind or radiative forcing and can be dampened by heat release from the sea surface (Hasselmann, 1976). Although the SHF anomalies are the main driver of the SST anomalies in most of the cases investigated here, in some cases MLD anomalies contribute more to the SST anomalies than the SHF anomalies. For example, FDA around Hawaii on June 2015 (Figure 1d) had positive values greater than 90˚ (i.e., light reddish color shading), suggesting that the SST anomalies were primarily determined by the "Q_H Growth" process rather than "Q_Q Growth" and "Q_Q Decay". In the next subsection, we further explore the regional and seasonal characteristics of the "Q_H Growth" and "Q_H Decay" processes.

3.2 Regional and seasonal characteristics of FDA

Figure 2 shows the FDA histograms for each ocean basin (Pacific, Atlantic, and Indian Ocean), different regions (Northern Hemisphere [NH], Equatorial region [EQ], and Southern Hemisphere [SH]), and different seasons (December-January-February [DJF], March-April-May [MAM], June-July-August [JJA], and September-October-November [SON]). Maps of the occurrence frequency of the four sectors in each season are also shown in Figure 3. Hereafter, we will describe the details of the relative contributions of MLD anomalies ("Q_H Growth" and "Q_H Decay") compared to the contribution of SHF anomalies ("Q_Q Growth" and "Q_Q Decay"). The contribution of SHF anomalies is dominant all over the global ocean (Fig. 2a-h), especially in most of the extra-tropical regions and in winter (Fig. 3a,c,e,g,i,k,m,o).

3.2.1 Q_H Growth process

In the extra-tropics (Fig. 2a,b,f,g,h), the histograms show a clear seasonal difference between summer and winter. In the winter hemisphere (i.e., JJA in the NH and DJF in the SH), occurrence frequencies of "Q_Q Growth" and "Q_Q Decay" are larger than those of "Q_H Growth" and "Q_H Decay". While occurrence frequencies of "Q_Q Growth" and "Q_Q Decay" are also large in summer, however, occurrence frequency of "Q_H Growth" in spring and summer is clearly larger than in winter. This suggests that the contribution of MLD anomalies is more pronounced in the spring and summer seasons than in the winter season, which is consistent with previous research (Alexander et al., 2000; Alexander & Penland, 1996; Cronin et al., 2013; Elsberry & Garwood, 1978; Lanzante & Harnack, 1983). The "Q_H Growth" sector reflects the negative covariance between anomalies of SST and MLD under climatological heating. In this situation, MLD decreases with enhanced upper ocean stratification due to the increase in SST and/or

decrease in sea surface salinity (i.e., decrease in the surface water density). On the other hand, SST easily increases under a shallow MLD anomaly and climatological surface heating in the summer hemisphere. Thus, during summer, this positive feedback loop between MLD and SST anomalies can amplify the local SST anomalies.

As noted in the previous paragraph, the "Q_H Growth" sector is dominant in the summer hemisphere, particularly in the eastern part of the ocean basins (Fig. 3d,h,l,p). The region with a large contribution of MLD anomalies exhibits a horseshoe-like pattern, especially in the North Pacific (Fig. 3h,l). One reason for the large contribution of MLD anomalies is large variability of MLD anomalies in subtropical regions (Fig. S4a), particularly due to strong surface friction velocity in the subtropical Pacific (Zhu & Zhang, 2018). Another reason is a large value of the ratio of mean SHF to mean MLD in the North Pacific and Atlantic (> 50 ˚N in Fig. S4b), which is mainly due to the shallow climatological mean MLD under the strong climatological heating at the sea surface (Fig. S4c, d).

3.2.2 Q_H Decay process

While the contribution of SHF anomalies is dominant in most of the tropics (Fig. 2c,d,e), there is a small peak of occurrence frequency of "Q_H Decay" in the EQ Pacific in SON and DJF (Fig. 2c). The "Q_H Decay" sector reflects the positive covariance between anomalies of SST and MLD. A positive covariance is associated with upwelling processes. When upwelling is enhanced, SST decreases due to more intrusion of cold water from deeper levels. At the same time, temperature around the bottom of the mixed layer decreases more than at the surface. Thus, MLD shoals due to the enhanced stratification induced by anomalous upwelling. Analogous, when upwelling is suppressed, SST increases due to less intrusion of cold water from deeper levels. At the same time, temperature around the bottom of the mixed layer increases more than at the surface. Thus, MLD becomes thicker due to less stratification induced by suppressed upwelling.

Horizontal maps of the "Q_H Decay" occurrence frequency (Fig. 3b,f,j,n) show that this process is dominant in the eastern tropical Pacific. As explained in the previous paragraph, it is consistent with the unique regionality of positive covariance between anomalies of SST and MLD due to the oceanic upwelling zone (Carton et al., 2008; Cronin & Kessler, 2002; Huang et al., 2012; Wang & McPhaden, 2000), resulting in negative anomalies of equivalent heat flux with deeper MLD under climatological heating in the tropics that act to dampen SST anomalies.

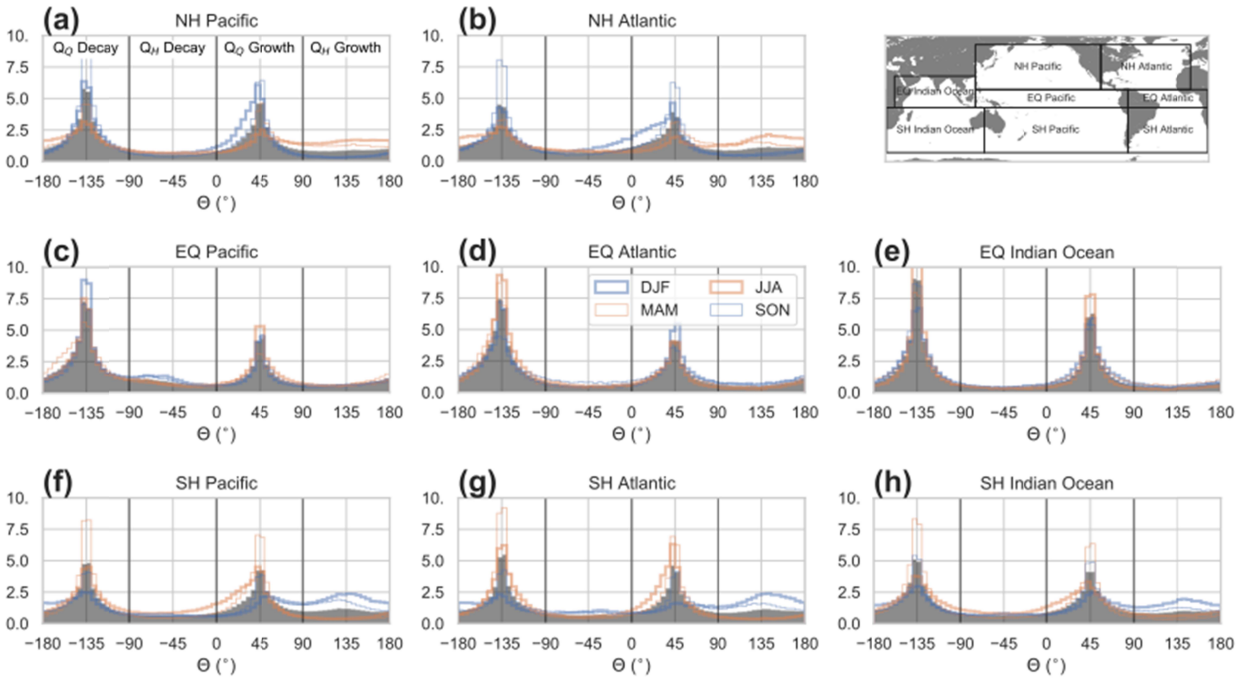

Figure 2: Normalized histograms of FDA in 8 selected regions (a. NH Pacific [120˚E-100˚W, 10˚N-60˚N], b. NH Atlantic [160˚W-0˚E, 10˚N-60˚N], c. EQ Pacific [120˚E-70˚W, 10˚S-10˚N], d. EQ Atlantic [70˚W-20˚E, 10˚S-10˚N], e. EQ Indian Ocean [30˚E-120˚E, 10˚S-25˚N], f. SH Pacific [130˚E-70˚W, 60˚S-10˚S], g. SH Atlantic [70˚W-20˚E, 10˚S-10˚N], and h. SH Indian Ocean [20˚E-130˚E, 60˚S-10˚S]). Each color and line width indicates the results for each season separately (DJF [thick, blue], MAM [thin, orange], JJA [thick orange], SON [thin blue], All season [black filled]). Bin size of the histograms is 5˚. Vertical lines in each panel indicates the boundary between each sector. The map in upper right corner indicates the area of each selected region.

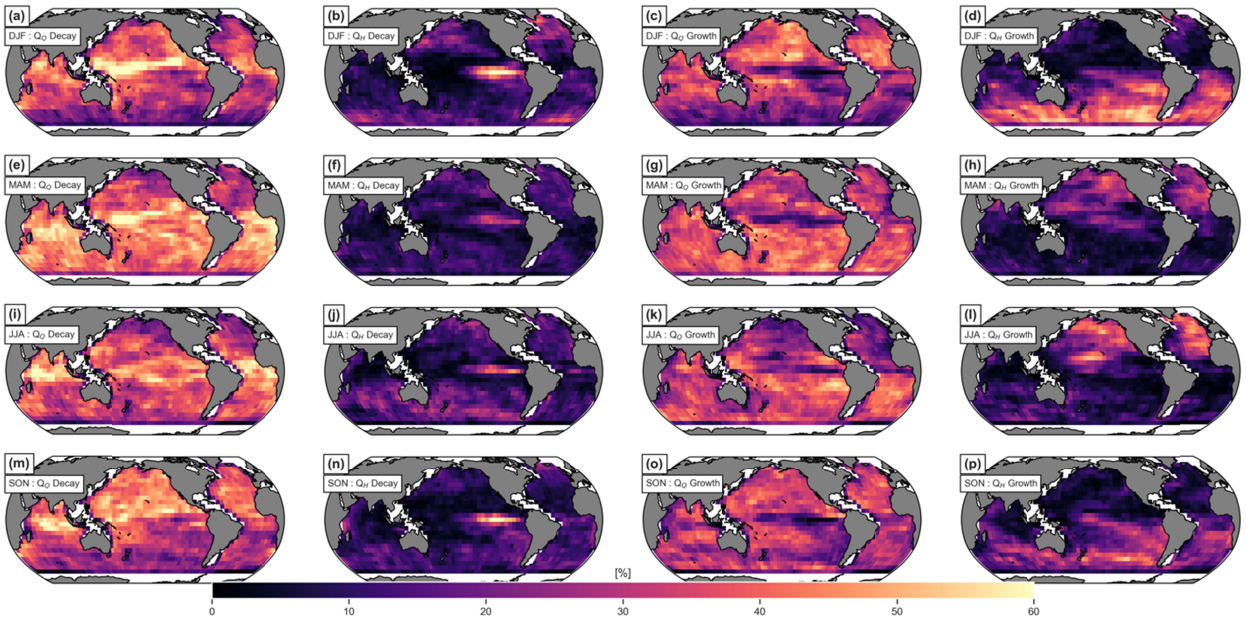

Figure 3: Horizontal maps of occurrence frequencies (Unit: %) in the four sectors for each season. From left to right, the "Q_Q Decay", "Q_H Decay", "Q_Q Growth", and "Q_H Growth" sectors are displayed, respectively. Each row shows the results in DJF (1st row), MAM (2nd row), JJA (3rd row), and SON (4th row).

3.3 Timescale dependence of the FDA histograms

Finally, we examine the timescale dependence of the relative contributions of SHF and MLD anomalies using 5-day mean variables from the SODA 3.4.2 dataset. Focusing on the summertime extra-tropics, when and where MLD anomalies largely contribute to the growth of the SST anomaly (Figs. 2 and 3), we compute the FDA histograms using low-pass filtered variables with different moving window sizes ranging from 15-days to 95-days (Fig. 4). The results show a clear timescale dependence of the dominant sectors, particularly for "Q_H Growth" (i.e., $90° < \Theta < 180°$). The contribution of the MLD anomaly is very small when no low-pass filtering is used (i.e., 5-day mean variable). However, the occurrence frequency of "Q_H Growth" becomes large when the window size is 25-days or 35-days in all selected regions and seasons. For example, in the summertime North Pacific (Fig. 4a), the occurrence frequency of "Q_H Growth" increases from 18.7 % to 27.8% and the occurrence frequency of "Q_Q Growth" decreases from 31.3 % to 22.6 % when we change the window size from 5-days to 35-days.

This suggests that contribution of MLD anomalies is more pronounced on seasonal timescales than on sub-monthly timescales. This could be explained by the difference in dominant frequencies between MLD and SHF variability. Specifically, the spectra of SHF and MLD anomalies correspond to "white noise" and "red noise", respectively (Fig. S5). Therefore, the contribution of MLD anomalies is more pronounced on longer timescales. Compared to the extra-tropics in the summer hemisphere, there is no clear timescale dependence of the contribution of MLD anomalies in the tropics (Fig. S6).

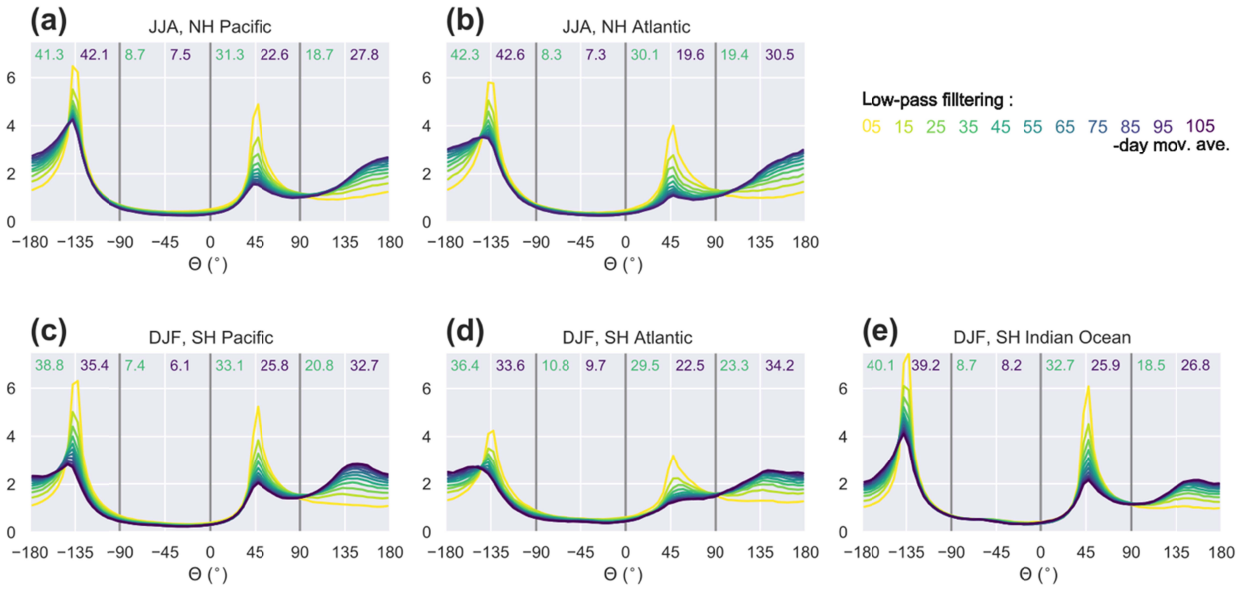

Figure 4: Timescale dependence of the FDA histograms in the extra-tropics in the summer hemisphere (JJA in NH and DJF in SH) using 5-day mean variables from SODA3.4.2. Colored lines show the histogram using different moving averaged variables in the time dimension (legend in the upper right corner of the panel). Colored text (light green and dark purple) at the top of each panel shows the relative frequencies in the four sectors using 5-day and 35-day mean variables, respectively (Unit: %).

4 Summary and Discussion

To reveal the seasonal and regional characteristics of the role of MLD anomalies in modulating SST variability, we propose a metric called Flux Divergence Angle (FDA) that quantifies the relative contributions of anomalies of SHF and MLD anomalies to the month-to-month variations of SST anomalies. The FDA is based on a metric proposed by Tozuka et al. (2018). Using the FDA, we investigate the seasonal and regional characteristics of their relative contributions. The contribution of MLD anomalies has two distinct features. First, MLD anomalies amplify local SST anomalies particular in the extra-tropics during spring and summer, relative to the contribution of SHF anomalies. Second, MLD anomalies suppress SST anomalies particularly in the eastern part of the tropical Pacific during DJF. As discussed in section 3, we speculate that the opposite role of MLD anomalies is associated with opposite signed covariances between SST and MLD anomalies due to different formation mechanisms of MLD (i.e., shoaling MLD by enhanced surface heating in the summertime extra-tropics *vs.* deepening MLD by enhanced upwelling in the eastern tropical Pacific). A timescale dependence of contributions of MLD anomalies in the extra-tropics during summer is also examined, indicating an enhanced contribution of MLD anomalies on seasonal timescales compared to sub-monthly timescales due to a large variance of MLD anomalies on longer timescales (red spectrum).

Our results show that the spatial pattern with pronounced contributions of MLD anomalies in the North Pacific during summer is horseshoe-like (Fig. 3). This implies that MLD anomalies might play a critical role in driving major climate modes in the North Pacific, such as the Pacific Decadal Oscillation (PDO). Recent papers pointed out the importance of MLD

anomalies in modulating major modes of climate variability such as the PDO (Dawe & Thompson, 2007), Atlantic Meridional Mode (Kataoka et al., 2019), and the Atlantic Multidecadal Oscillation (Yamamoto et al., 2020). Kataoka et al. (2019) also revealed that variations in MLD have the potential to more than double the wind-evaporation-SST feedback rate. Thus, the role of MLD anomalies in climate variability should be paid more attention to and its further investigation is needed. In addition, large uncertainties associated with summertime MLD in ocean and coupled general circulation models have been found (Ezer, 2000; Huang et al., 2014) which is a potential source of SST biases (Zhu et al., 2020). Thus, improved understanding of different formation mechanisms of MLD anomalies is required, especially for physical processes associated with the atmospheric-forced MLD variability (Lee et al., 2015; Pookkandy et al., 2016; Ushijima & Yoshikawa, 2019; Yoshikawa, 2015). Finally, we note that our simple metric based on only three variables appears to be a useful diagnostic of the upper ocean representation in climate models.

Data Availability Statement

Most of the datasets used in this study can be downloaded from Asia-Pacific Data Research Center; http://apdrc.soest.hawaii.edu/data/data.php, which is a part of the International Pacific Research Center at the University of Hawai‘i at Mānoa, funded in part by the National Oceanic and Atmospheric Administration (NOAA). Original data sources are listed below; OISSTv2 is from https://www.ncei.noaa.gov/products/optimum-interpolation-sst, SODA3.4.2 dataset is from https://www2.atmos.umd.edu/~ocean/index_files/soda3.4.2_mn_download_b.htm. CERES data were obtained from the NASA Langley Research Center CERES ordering tool at https://asdc.larc.nasa.gov/project/CERES/CERES_EBAF_Edition4.1. The global ocean heat flux and evaporation data provided by the Woods Hole Oceanographic Institution OAFlux project (https://oaflux.whoi.edu/data-access/) were funded by the NOAA Climate Observations and Monitoring (COM) program.

Acknowledgments

This study was supported by the collaborative JICore project between JAMSTEC and IPRC. MFS was supported by NSF grant AGS-2141728 and NOAA’s Climate Program Office’s Modeling, Analysis, Predictions, and Projections (MAPP) program grant NA20OAR4310445. HA acknowledges the partial support from NOAA/MAPP program grants NA18OAR4310279 and NA21OAR4310348. This is IPRC publication X and SOEST contribution Y.

References

Alexander, M. A., & Penland, C. (1996). Variability in a Mixed Layer Ocean Model Driven by Stochastic Atmospheric Forcing. *Journal of Climate*, *9*(10), 2424–2442. https://doi.org/10.1175/1520-0442(1996)009<2424:VIAMLO>2.0.CO;2

Alexander, M. A., Scott, J. D., & Deser, C. (2000). Processes that influence sea surface temperature and ocean mixed layer depth variability in a coupled model. *Journal of Geophysical Research: Oceans*, *105*(C7), 16823–16842. https://doi.org/10.1029/2000jc900074

Amaya, D. J., Alexander, M. A., Capotondi, A., Deser, C., Karnauskas, K. B., Miller, A. J., & Mantua, N. J. (2021). Are Long-Term Changes in Mixed Layer Depth Influencing North Pacific Marine Heatwaves? *Bulletin of the American Meteorological Society*, *102*(1), S59–S66. https://doi.org/10.1175/BAMS-D-20-0144.1

Boucharel, J., Timmermann, A., Santoso, A., England, M. H., Jin, F., & Balmaseda, M. A. (2015). A surface layer variance heat budget for ENSO. *Geophysical Research Letters*, *42*(9), 3529–3537. https://doi.org/10.1002/2015GL063843

de Boyer Montégut, C. (2004). Mixed layer depth over the global ocean: An examination of profile data and a profile-based climatology. *Journal of Geophysical Research*, *109*(C12), C12003. https://doi.org/10.1029/2004JC002378

Carton, J. A., Grodsky, S. A., & Liu, H. (2008). Variability of the oceanic mixed layer, 1960-2004. *Journal of Climate*, *21*(5), 1029–1047. https://doi.org/10.1175/2007JCLI1798.1

Carton, J. A., Chepurin, G. A., & Chen, L. (2018). SODA3: A New Ocean Climate Reanalysis. *Journal of Climate*, *31*(17), 6967–6983. https://doi.org/10.1175/JCLI-D-18-0149.1

Cronin, M. F., & Kessler, W. S. (2002). Seasonal and interannual modulation of mixed layer variability at 0°, 110°W. *Deep Sea Research Part I: Oceanographic Research Papers*, *49*(1), 1–17. https://doi.org/10.1016/S0967-0637(01)00043-7

Cronin, M. F., Bond, N. A., Thomas Farrar, J., Ichikawa, H., Jayne, S. R., Kawai, Y., et al. (2013). Formation and erosion of the seasonal thermocline in the Kuroshio Extension

Recirculation Gyre. *Deep Sea Research Part II: Topical Studies in Oceanography*, *85*, 62–74. https://doi.org/10.1016/j.dsr2.2012.07.018

Dawe, J. T., & Thompson, L. A. (2007). PDO-Related Heat and Temperature Budget Changes in a Model of the North Pacific. *Journal of Climate*, *20*(10), 2092–2108. https://doi.org/10.1175/JCLI4229.1

Dee, D. P., Uppala, S. M., Simmons, A. J., Berrisford, P., Poli, P., Kobayashi, S., et al. (2011). The ERA-Interim reanalysis: configuration and performance of the data assimilation system. *Quarterly Journal of the Royal Meteorological Society*, *137*(656), 553–597. https://doi.org/10.1002/qj.828

Elsberry, R. L., & Garwood, R. W. (1978). Sea-Surface Temperature Anomaly Generation in Relation to Atmospheric Storms. *Bulletin of the American Meteorological Society*, *59*(7), 786–789. https://doi.org/10.1175/1520-0477(1978)059<0786:SSTAGI>2.0.CO;2

Ezer, T. (2000). On the seasonal mixed layer simulated by a basin-scale ocean model and the Mellor-Yamada turbulence scheme. *Journal of Geophysical Research: Oceans*, *105*(C7), 16843–16855. https://doi.org/10.1029/2000JC900088

Frankignoul, C., & K. Hasselmann. (1977). Stochastic Climate Models, Part II Application to Sea-Surface Temperature Anomalies and Thermocline Variability. *Tell'Us*, *29* (4), 289–305.

Guan, C., McPhaden, M. J., Wang, F., & Hu, S. (2019). Quantifying the Role of Oceanic Feedbacks on ENSO Asymmetry. *Geophysical Research Letters*, *46*(4), 2140–2148. https://doi.org/10.1029/2018GL081332

Hasselmann, K. (1976). Stochastic Climate Models Part I. Theory. *Tell'Us,* 28 (6), 473–85.

Huang, B., Xue, Y., Wang, H., Wang, W., & Kumar, A. (2012). Mixed layer heat budget of the El Niño in NCEP climate forecast system. *Climate Dynamics*, *39*(1–2), 365–381.

https://doi.org/10.1007/s00382-011-1111-4

Huang, C. J., Qiao, F., & Dai, D. (2014). Evaluating CMIP5 simulations of mixed layer depth during summer. *Journal of Geophysical Research: Oceans*, *119*(4), 2568–2582. https://doi.org/10.1002/2013JC009535

Kataoka, T., Kimoto, M., Watanabe, M., & Tatebe, H. (2019). Wind–Mixed Layer–SST Feedbacks in a Tropical Air–Sea Coupled System: Application to the Atlantic. *Journal of Climate*, *32*(13), 3865–3881. https://doi.org/10.1175/JCLI-D-18-0728.1

Lanzante, J. R., & Harnack, R. P. (1983). An investigation of summer sea surface temperature anomalies in the eastern North Pacific Ocean. *Tellus A: Dynamic Meteorology and Oceanography*, *35*(4), 256–268. https://doi.org/10.3402/tellusa.v35i4.11438

Lee, E., Noh, Y., Qiu, B., & Yeh, S.-W. (2015). Seasonal variation of the upper ocean responding to surface heating in the North Pacific. *Journal of Geophysical Research: Oceans*, *120*(8), 5631–5647. https://doi.org/10.1002/2015JC010800

Loeb, N. G., Doelling, D. R., Wang, H., Su, W., Nguyen, C., Corbett, J. G., et al. (2018). Clouds and the Earth's Radiant Energy System (CERES) Energy Balanced and Filled (EBAF) Top-of-Atmosphere (TOA) Edition-4.0 Data Product. *Journal of Climate*, *31*(2), 895–918. https://doi.org/10.1175/JCLI-D-17-0208.1

Morioka, Y., Tozuka, T., & Yamagata, T. (2010). Climate variability in the southern Indian Ocean as revealed by self-organizing maps. *Climate Dynamics*, *35*(6), 1059–1072. https://doi.org/10.1007/s00382-010-0843-x

Morioka, Y., Tozuka, T., & Yamagata, T. (2011). On the Growth and Decay of the Subtropical Dipole Mode in the South Atlantic. *Journal of Climate*, *24*(21), 5538–5554. https://doi.org/10.1175/2011JCLI4010.1

435 Paulson, C. A., & Simpson, J. J. (1977). Irradiance Measurements in the Upper Ocean. *Journal*
436 *of Physical Oceanography*, *7*(6), 952–956. https://doi.org/10.1175/1520-
437 0485(1977)007<0952:IMITUO>2.0.CO;2
438 Pookkandy, B., Dommenget, D., Klingaman, N., Wales, S., Chung, C., Frauen, C., & Wolff, H.
439 (2016). The role of local atmospheric forcing on the modulation of the ocean mixed layer
440 depth in reanalyses and a coupled single column ocean model. *Climate Dynamics*, *47*(9–10),
441 2991–3010. https://doi.org/10.1007/s00382-016-3009-7
442 Qiu, B., & Kelly, K. A. (1993). Upper-Ocean Heat Balance in the Kuroshio Extension Region.
443 *Journal of Physical Oceanography*, *23*(9), 2027–2041. https://doi.org/10.1175/1520-
444 0485(1993)023<2027:UOHBIT>2.0.CO;2
445 Reynolds, R. W., Rayner, N. A., Smith, T. M., Stokes, D. C., & Wang, W. (2002). An Improved
446 In Situ and Satellite SST Analysis for Climate. *Journal of Climate*, *15*(13), 1609–1625.
447 https://doi.org/10.1175/1520-0442(2002)015<1609:AIISAS>2.0.CO;2
448 Ruddick, B. (1983). A practical indicator of the stability of the water column to double-diffusive
449 activity. *Deep Sea Research Part A. Oceanographic Research Papers*, *30*(10), 1105–1107.
450 https://doi.org/10.1016/0198-0149(83)90063-8
451 Santoso, A., Sen Gupta, A., & England, M. H. (2010). Genesis of Indian Ocean Mixed Layer
452 Temperature Anomalies: A Heat Budget Analysis. *Journal of Climate*, *23*(20), 5375–5403.
453 https://doi.org/10.1175/2010JCLI3072.1
454 Sugimoto, S., & Kako, S. (2016). Decadal Variation in Winter Mixed Layer Depth South of the
455 Kuroshio Extension and Its Influence on Winter Mixed Layer Temperature. *Journal of*
456 *Climate*, *29*(3), 1237–1252. https://doi.org/10.1175/JCLI-D-15-0206.1
457 Takahashi, N., Richards, K. J., Schneider, N., Annamalai, H., Hsu, W., & Nonaka, M. (2021).

458 Formation Mechanism of Warm SST Anomalies in 2010s Around Hawaii. *Journal of*
459 *Geophysical Research: Oceans*, *126*(11), 1–14. https://doi.org/10.1029/2021JC017763
460 Tozuka, T., S. Ohishi, and M. F. Cronin. (2018). A Metric for Surface Heat Flux Effect on
461 Horizontal Sea Surface Temperature Gradients., *Climate Dynamics,* 51 (1–2), 547–61
462 Ushijima, Y., & Yoshikawa, Y. (2019). Mixed Layer Depth and Sea Surface Warming under
463 Diurnally Cycling Surface Heat Flux in the Heating Season. *Journal of Physical*
464 *Oceanography*, *49*(7), 1769–1787. https://doi.org/10.1175/JPO-D-18-0230.1
465 Wang, W., & McPhaden, M. J. (2000). The surface-layer heat balance in the Equatorial Pacific
466 Ocean Part II: Interannual variability. *Journal of Physical Oceanography*, *30*(11), 2989–
467 3008. https://doi.org/10.1175/1520-0485(2001)031<2989:TSLHBI>2.0.CO;2
468 Yamaguchi, R., & Suga, T. (2019). Trend and Variability in Global Upper-Ocean Stratification
469 Since the 1960s. *Journal of Geophysical Research: Oceans*, *124*(12), 8933–8948.
470 https://doi.org/10.1029/2019JC015439
471 Yamamoto, A., Tatebe, H., & Nonaka, M. (2020). On the Emergence of the Atlantic
472 Multidecadal SST Signal: A Key Role of the Mixed Layer Depth Variability Driven by
473 North Atlantic Oscillation. *Journal of Climate*, *33*(9), 3511–3531.
474 https://doi.org/10.1175/JCLI-D-19-0283.1
475 Yokoi, T., Tozuka, T., & Yamagata, T. (2012). Seasonal and Interannual Variations of the SST
476 above the Seychelles Dome. *Journal of Climate*, *25*(2), 800–814.
477 https://doi.org/10.1175/JCLI-D-10-05001.1
478 Yoshikawa, Y. (2015). Scaling surface mixing/mixed layer depth under stabilizing buoyancy
479 flux. *Journal of Physical Oceanography*, *45*(1), 247–258. https://doi.org/10.1175/JPO-D-
480 13-0190.1

You, Y. (2002). A global ocean climatological atlas of the Turner angle: implications for double-diffusion and water-mass structure. *Deep Sea Research Part I: Oceanographic Research Papers*, *49*(11), 2075–2093. https://doi.org/10.1016/S0967-0637(02)00099-7

Yu, L., Jin, X., & Robert, A. W. (2008). *Multidecade Global Flux Datasets from the Objectively Analyzed Air-sea Fluxes (OAFlux) Project: Latent and Sensible Heat Fluxes, Ocean Evaporation, and Related Surface Meteorological Variables*. *Woods Hole Oceanographic Institution OAFlux Project Technical Report (OA-2008-01)*. https://doi.org/10.1007/s00382-011-1115-0

Zhu, Y., & Zhang, R.-H. (2018). Scaling wind stirring effects in an oceanic bulk mixed layer model with application to an OGCM of the tropical Pacific. *Climate Dynamics*, *51*(5–6), 1927–1946. https://doi.org/10.1007/s00382-017-3990-5

Zhu, Y., Zhang, R.-H., & Sun, J. (2020). North Pacific Upper-Ocean Cold Temperature Biases in CMIP6 Simulations and the Role of Regional Vertical Mixing. *Journal of Climate*, *33*(17), 7523–7538. https://doi.org/10.1175/JCLI-D-19-0654.1

496